Results in Engineering 32 (2026) 112294

Contents lists available at ScienceDirect

Results in Engineering

journal homepage: www.sciencedirect.com/journal/results-in-engineering

Research paper

# A comminution chain for lithium-bearing slags as artificial minerals using roller mills

Sima Hellmers [a,*], Hugo Lucas [b], Bernd Friedrich [b], Arno Kwade [a]

[a] Institute for Particle Technology (iPAT), Technische Universität Braunschweig, Volkmaroderstr. 5, 38104, Braunschweig, Germany
[b] Institute of Process Metallurgy and Metal Recycling (IME), RWTH Aachen University, Intzestr. 3, 52056, Aachen, Germany

ARTICLE INFO

*Keywords:*
Engineered lithium-bearing slags
Comminution processes
Compressive stressing
Roller mills
Circuit milling

ABSTRACT

Efficient recovery of lithium from secondary sources, such as pyrometallurgical battery slags, remains a major challenge with significant environmental and resource implications. This study develops and evaluates a scalable comminution process chain for engineered lithium-rich slags, emphasizing energy-efficient grinding toward a flotation-ready product (<100 μm). Impact- and compression-based mills were compared with respect to breakage mechanisms, particle-size evolution, and specific energy demand for crushing. Fine grinding was subsequently conducted in a rigidly mounted roller mill, where roller-gap variation was systematically analyzed to optimize particle-size distribution and energy consumption.

Energy efficiency was quantified using size-specific energy and energy utilization. Compression stressing produced narrower particle-size distributions and higher energy efficiency, with the most energy-effective performance observed at moderate gap ratios of 40% of the median size of feed. In contrast, impact stressing generated broader distributions dominated by shattering but facilitated early liberation of metallic droplets from the slag matrix. Continuous grinding experiments in series and circuit modes demonstrated that circuit operations achieved up to 20% lower energy demand by preventing redundant stressing of fines, whereas series milling achieved higher mass yield for the same throughput and number of stress events. The proposed hybrid process chain, combining impact pre-crushing with staged roller milling, provides a mechanistic framework for designing energy-efficient dry-grinding circuits and supports scalable lithium recovery from complex slags.

## 1. Introduction

The extraction and recovery of valuable metals from secondary sources such as pyrometallurgical recycling slags address both environmental challenges and resource sustainability concerns [1–4]. Among these residues, lithium-bearing slags— by-products of the pyrometallurgical treatment of spent lithium-ion batteries (LIBs)—represent a promising secondary source for lithium recovery [5–7]. Global demand for lithium is rapidly increasing due to the growth of the electric vehicle and energy storage sectors, intensifying the need for sustainable and efficient recycling routes [8,9]. The complex multiphase composition of these slags makes efficient recovery of lithium challenging, necessitating efficient comminution and phase-liberation strategies [10, 9].

Thermodynamic design of lithium-bearing slags offers a route to tailor phase groupings and stabilize γ-$LiAlO_2$, a lithium-rich phase amenable to downstream flotation [11]. By adjusting the $CaO–Al_2O_3–SiO_2–Li_2O$ systems, slags can be engineered into artificial minerals whose breakage and separation behavior resemble those of conventional ores [12–15]. This concept—engineering slags for enhanced comminution and liberation—forms the foundation of the present work.

In the recycling of lithium-ion batteries, comminution is essential for breaking down battery components to facilitate the subsequent separation and recovery of valuable materials such as lithium, cobalt, and nickel. This process not only aids in the efficient recycling of these materials but also contributes to the sustainability of battery production by reducing the need for primary raw material ( [6,16]. Similarly, comminution is a critical and energy-intensive step in mineral processing that strongly affects liberation efficiency and overall process economics. In the broader context of metallurgical slags, comminution facilitates the recovery of valuable metals and other elements. The separation methods such as flotation or innovative method of dry forced triboelectric separation implemented in lithium recovery from slag,

* Corresponding author.
*E-mail address:* s.hellmers@tu-braunschweig.de (S. Hellmers).

https://doi.org/10.1016/j.rineng.2026.112294
Received 8 December 2025; Received in revised form 17 February 2026; Accepted 31 July 2026
Available online 1 August 2026
2590-1230/© 2026 The Authors. Published by Elsevier B.V. This is an open access article under the CC BY license (http://creativecommons.org/licenses/by/4.0/).

underscore the importance of comminution in advancing sustainable recycling practices [17]. Overall, comminution is integral to the slag industry, enabling efficient resource recovery and contributing to environmental sustainability. Thus, selecting appropriate comminution processes minimizes the stream of gangue minerals in separation and increases the recovery rate of the target phases [18]. Compared with conventional ores, slags require finer particle sizes for effective separation and therefore consume more energy [19,20]. The heterogeneous composition of slags, containing a mixture of metallic and ceramic materials with similar physical properties, necessitates customized milling conditions [14]. However, previous studies have largely overlooked a comparison of the impact and compressive stressing mechanisms on the breakage, energy efficiency, and liberation of lithium phases in slags.

The precise control of product fineness depends on the type of stress applied to the particles, the medium of milling, and the fracture mechanism of the particles. In comminution theory, two primary stress mechanisms dominate: impact stressing, a high-energy single-event breakage producing broad size distributions, and compressive stressing, a lower-energy, repetitive event yielding more uniform particles [21–25, 20]. The choice between wet and dry grinding further influences performance; dry grinding routes often offer environmental and operational advantages for slag processing. Conversely, in most ore processing plants, ores are milled wet to produce a slurry for downstream separation through hydro cyclones and flotation techniques, these steps can be replaced with dry grinding [26–28].

To address this gap, the present study develops and evaluates a comminution process chain for lithium-bearing slags. The objective is to design a simple yet robust process that achieves efficient particle liberation with minimal operating parameters. Roller mills—characterized by structural simplicity, low maintenance, and high grinding efficiency compared with ball mills—are employed as the core equipment. Their use simplifies process design and prevents overgrinding, which can hinder subsequent hydrometallurgical leaching steps [29–32]. These mills can achieve a multi-stage milling process by adjusting the gap size and circumferential speed of the rollers according to the size of the feed particles. Complementary to grinding in roller mills, stirred media mills can be used as an additional comminution step to support hydrometallurgical processes. This approach enhances the solubility of lithium-bearing phases, thereby, reducing the need for leaching reagents in subsequent hydrometallurgical processes [33].

Despite recent interest and the importance of slag comminution for lithium recovery, a comprehensive evaluation of diverse grinding techniques and their impact on particle characteristics is still lacking. Therefore, to improve the effectiveness of slag comminution methodologies, this study investigates the comminution behavior of a lithium-bearing battery slag from crushing to fine grinding, that is from macroscopic to microscopic levels. To this end, this study analyzes the particle size evolution and specific breakage energy under impact and compressive stress. Regarding energy and flotation efficiency, this study focuses on designing a process chain that mainly implements roller mills. The advantage of these mills is their simple design, and the lack of necessity for grinding media, grinding aids, and waste management. Controlling these mills is also limited to the three primary grinding parameters of circumferential speed, throughput, and roller gap size [32,34]. These properties make roller mills a suitable option for slag grinding. To provide a more thorough evaluation of roller mills' ability to operate continuously at industrial scale, the research proposes two subsequent grinding steps applying compressive stress. These processes are examined for stress events and the subsequent breakage energy of grinding, with the potential to investigate liberation efficiency of lithium-containing phases in the future. By identifying the most energy-efficient grinding configuration, this study contributes to the development of sustainable process designs for battery recycling.

## 2. Materials and methods

### 2.1. Materials

The material used in this study was a lithium-bearing slag derived from the pyrometallurgical recycling of end-of-life (EoL) pyrolyzed lithium batteries with lithium nickel manganese cobalt oxides (NMC) as cathode material. This slag was produced in a pilot-scale facility in the Institute of Process Metallurgy and Metal Recycling (IME), RWTH Aachen University, aimed at converting lithium present in the feed into the desired γ-$LiAlO_2$ phase [14,15].

The synthesis of the slag was conducted in a medium-sized top-blown rotary converter (TBRC) with a 300 L vessel, operated with natural gas and oxygen as fuel sources. A total of 187.5 kg of EoL pyrolyzed NMC batteries provided by Accurec Recycling GmbH were used. The following additives were used to tailor the slag composition: 14.5 kg quartz (Quarzwerke GmbH, Frechen, Germany), 21.75 kg calcined lime (Weissfeinkalk CL 90, Dyckerhoff GmbH, Germany), 26.25 kg calcined $Al_2O_3$ (Almatis GmbH, Germany), $SiO_2$ (IOTA, Sibelco N.V., Belgium), 18.75 kg copper (II) oxide (Lomberg GmbH, Oberhausen, Germany) with a CuO content exceeding 98.9 wt.%. A combustion lambda of 1.05 (indicating a stoichiometric excess of oxygen) was used to combust part of the 21 wt.% of graphite in the batteries. After processing the batteries in the Midi-TBRC at temperatures of approximately 1500 °C, the molten mass was transferred to a preheated electric furnace at 1350 °C (IME Doppelofen Thermo-Star GmbH) and cooled at a controlled rate of 25 °C/h. Within the confines of the furnace, a Mars-uniCstar KK600 (67 l working volume) graphite crucible from Aug-Gundlach GmbH was used. This slag was subsequently characterized to identify the most prominent lithium-bearing phases, which are critical for understanding possible breakage mechanisms.

Table 1 presents the elemental analysis of the batteries used in the experiment and the obtained slag. The measurements were conducted with a "Spectro CIROS Vision" inductively coupled plasma-optical emission spectrometer (ICP-OES) produced by SPECTRO Analytical Instruments GmbH, Kleve, Germany. Carbon content was measured using the combustion method with an ELTRA CS 2000 system designed by ELTRA GmbH, Haan, Germany. The mineralogical composition of the slag was determined by Rietveld analysis as described in details by Li et al. [13]. This analysis was instrumental in identifying the most prominent lithium-containing phases, which are critical in understanding the possible breakage mechanisms.

### 2.2. Comminution processes

This study aimed to propose a scalable comminution chain accommodating the complex, multiphase structure of battery slags. Fig. 1a shows the process design, comprising four stages: primary crushing, secondary crushing, grinding, and metal recovery via hydrometallurgy. These stages covered the entire process chain, from comminution to recovery of the lithium. Prior to crushing, the lithium-bearing slag block was mechanically cut into twelve parts to facilitate handling and ensure homogeneous subdivision of the material. Three parts constituting one-quarter of the slag formed one sample, which were processed separately to provide representative material for subsequent experiments. Primary crushing was conducted using a jaw crusher (Nordberg C100, Metso, Finland). Each quarter was passed through the crusher four times until a top particle size below approximately 10 mm was achieved. The nominal nip angle of the crusher is approximately 20°, according to manufacturer specifications. The crushed material was sieved using a sieve shaker (AS 200 control, Retsch, Germany) at 1.8 mm amplitude for five minutes. For fractions $< 200$ μm, an air jet sieve (Hosokawa-Alpine, Germany) was used to reduce the fines in the investigated size classes. The present study focused on secondary crushing and fine grinding. To assess scalability, two continuous operational modes—circuit and series operation—were designed for the roller mill tests (Fig. 1b), focusing on

**Table 1**
a) Elemental composition of End-of-life pyrolyzed NMC batteries and resulting slag. b) Phase composition of the slag determined by Rietveld analysis.

| a) | | Al | Co | Cr | Cu | Fe | Li | Mn | Ni | Si | F | C |
|---|---|---|---|---|---|---|---|---|---|---|---|---|
| LIBs | wt.% | 5.8 | 3.7 | 0.4 | 9.3 | 19.9 | 2.8 | 12.3 | 10.3 | 0.1 | 1.9 | 21.4 |
| Slag | wt.% | 19.2 | 0.1 | 0.3 | 0.3 | 0.4 | 4.0 | 3.8 | 0.2 | 4.7 | 1.4 | 1.7 |
| b) | | | | | | | | | | | | |
| Composition | **$Ca_2Al_2SiO_7$** | **β- $LiAlSiO_4$** | **γ-$LiAlO_2$** | **$Li_2MnSiO_4$** | **$Li_xMn_{1-2x}Al_{2+x}O_8$** | **Graphite** | **$Ca_8[F_4(Si_2O_7)_2]$** | | | | | |
| (wt.%) | 13.4 | 2.1 | 43.9 | 2.2 | 22.3 | 5.2 | 10.9 | | | | | |

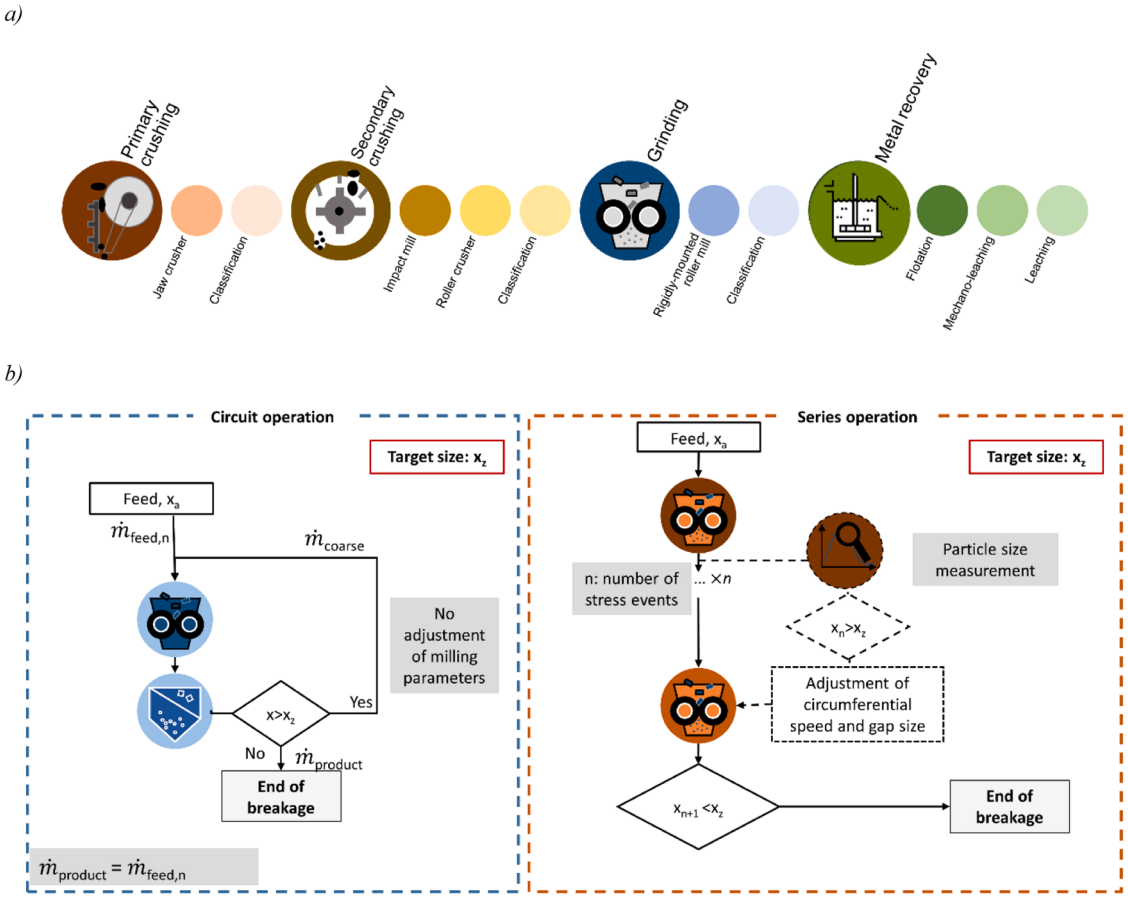


**Fig. 1.** a) Process chain designed for lithium recovery from battery slags; b) Two operational modes for continuous grinding in rigidly mounted roller mills, demonstrating scalability with circuit and series operations.

input energy efficiency and throughput. The subsequent metal recovery with flotation and leaching have been discussed in previous studies [12, 35].

### 2.2.1. *Impact mill*

Impact stressing was investigated using an impact mill (No. 9459, Hazemag, Dülmen, Germany) with four fixed impact bars. The rotor had a diameter of 288 mm and a constant circumferential speed of 21.1 m/s. For each run, 200 g of feed was milled at 20 °C. Product fractions (1.5 - 2.5 mm, 3.0 - 6.0 mm, and 7.0 - 10.0 mm) were obtained by sieving. The crushed product exited the mill unscreened and was subsequently sieved to remove fines and prepare the material for subsequent grinding processes.

### 2.2.2. *Roller crusher*

Compressive stressing was investigated using a roller crusher (WS 250 × 150 L, Siebtechnik Tema, Germany) on the same three coarse size classes. For each fraction, the circumferential speed was set to match particle fall velocity from feed hopper to the roller surface. Based on previous studies [36,12], four gap sizes were chosen in relation to the median size of the feed size class (20, 30, 40, and 50% of the $x_{50,\ feed}$). Gap sizes of 20–50% of $x_{50,feed}$ were selected because larger gaps (>50%) are known to produce insufficient compression for effective single-particle fracture, resulting in only negligible PSD shifts ($x_{50,\ product}$>0.9 $x_{50,feed}$) and increase in the need for repeated comminution passes [28,37,20]. Below a relative gap size of 20%, the feed condition of the roller crusher or mill, respectively, are no longer fulfilled. These milling parameters are shown in detail in Table 2a.

### 2.2.3. *Rigidly-mounted roller mill*

Fine grinding was conducted in a rigidly mounted roller mill developed by Böttcher et al. [36] for size classes in the range of 100 - 200 μm, 200 – 350 μm, and 350 – 500 μm. Operating parameters were similar to those of the roller crusher and are listed in Table 2b with (30, 40, 50 and 60% of the median feed size. Since the maximum possible gap size was 180 μm, for the feed size of 417 μm, the gap sizes were set at 30%, 40% and 45% of the $x_{50,\ feed}$.

### 2.2.4. *Continuous milling*

Two continuous grinding strategies were investigated in the rigidly-

**Table 2**
Milling parameters for a) Roller crusher (crushing); b) Rigidly mounted roller mill (grinding).

a) Milling parameters with gap size variations in roller crusher (crushing)

| Fraction (mesh size in μm) | | 1500–2500 | 3000–6000 | 7000–10,000 |
|---|---|---|---|---|
| $x_{50}$ of feed (μm) | | 1765 | 4601 | 9405 |
| Gap sizes between the rolls relative to feed size (μm) | *20% of* $x_{50}$ | 300 | 900 | 2400 |
| | *30% of* $x_{50}$ | 500 | 1400 | 3600 |
| | *40% of* $x_{50}$ | 700 | 1800 | 4700 |
| | *50% of* $x_{50}$ | 800 | 2300 | 6600 |
| Circumferential speed (m/s) | | 1.7 | 1.8 | 1.9 |
| Mass flow of feed (g/s) | | 5.4 | 5.4 | 5.4 |

b) Milling parameters with gap size variations in rigidly-mounted roller mill (grinding)

| Fraction (mesh size in μm) | | 100–200 | 200–350 | 350–500 |
|---|---|---|---|---|
| $x_{50}$ of feed (μm) | | 174 | 304 | 417 |
| Gap sizes between the rolls relative to feed size (μm) | *30% of* $x_{50}$ | 52 | 91 | 125 |
| | *40% of* $x_{50}$ | 70 | 121 | 166 |
| | *50% of* $x_{50}$ | 87 | 152 | 180* |
| | *60% of* $x_{50}$ | 104 | 180* | - |
| Circumferential speed (m/s) | | 1.1 | 2.0 | 2.5 |
| Mass flow of feed (g/s) | | 0.2 | 0.4 | 0.5 |

* For this gap size the maximum possible gap size of the mill of 180 μm was chosen.

mounted roller mill to reach the flotation-ready particle size (< 100 μm). As shown in Fig. 1b, these modes demonstrate the potential for upscaling the processes, especially by implementing several mills with different settings operating at the same time.

Circuit operation

In this approach, a constant circumferential speed and gap size were selected based on the median size of the given feed. After each milling pass, the resulting products were sieved to separate the target fraction of < 100 μm. The separated fines were weighed, and new material (with the same particle size as the initial feed) was added to the coarse fraction in an amount equal to the mass of the removed fines and mixed with the remaining coarse product from sieving. This new mixture was then reintroduced to the mill with the same circumferential speed and gap size.

The grinding was repeated until a steady state was reached, where the mass of fines produced, the median size of the mixed material, and the specific grinding energy remained constant. In this study, three feed sizes with median sizes of 174, 304, and 417 μm, previously tested in the single-pass milling experiments, were investigated.

The first stress event was conducted with the same circumferential speed and with gap-size variations as shown in Table 2b The limited sample mass prevented the formation of a quantifiable fine fraction at 50% and 60% gap sizes, making these conditions unsuitable for meaningful analysis. Consequently, the study was restricted to the 30% and 40% gap sizes, reducing the range of operational settings that could be systematically compared. The stress events were repeated five times with the constant circumferential speed and the gap sizes given in Table 2b

Series operation

In this approach, the feed material was ground repeatedly without intermediate sieving until the target size of < 100 μm was achieved. After each pass and thus stress event, the particle-size distribution of the product was measured. Based on the updated median size, the circumferential speed and gap size of the roller mill were adjusted for the following pass.

In this study, the three feed-size classes were first milled with the parameter settings given in Table 2b After the first pass, the particle size of the product was measured. Based on the new median size and the initial gap-size setting, the milling parameters were adjusted for each pass. The relative gap size was kept constant: for a 30% variation, the new gap size was 30% of the new median size; for a 40% variation, the new gap size was 40% of the new median size and so on for the subsequent grinding events. The circumferential speed was recalculated after each pass using an empirical fit derived from calibration measurements performed for different feed sizes. Depending on the initial median size of the feed and the relative gap size, the stress events were repeated 3–6 times with adjusted milling parameters until the target $x_{90}$ = 100 μm was reached. In this operational mode, it was possible to investigate gap-size variations of 30%, 40%, 50%, and 60% of the (updated) median feed size for each stress event. Torque was measured to calculate the specific comminution energy. To ensure reproducibility, all experiments in the mills and crushers were repeated three times. The evaluation of cumulative specific energy, size-specific energy, and energy utilization as well as the measurements used to summarize and compare comminution performance, are described in detail in the Results and Discussion section in conjunction with the corresponding figures.

### 2.3. Analytical methods

In this section, different analytical methods implemented to provide the necessary data required in the calculations for comparing different stress modes, operation modes and efficiency of the designed process for the grinding of the slag particles in the roller mills are provided:

#### 2.3.1. Particle size measurement

The measurement of feed and product particles below 1000 μm was performed by laser diffraction analysis using a Mastersizer 3000 (Malvern Panalytical, UK) with a measuring range of 0.1 μm −2500 μm. All analyses were conducted in wet dispersion using distilled water. For particles above 1000 μm, a dynamic image analyzer (Litesizer DIA 500, Anton Paar, Germany) with a measuring range of 0.8 μm to 16,000 μm was used to determine particle size distribution since measurements with the Mastersizer were not possible for this range. For samples with particle sizes above 1000 μm, the entire sample (approximately 200 g) was analyzed by dynamic image analysis, and measurements were repeated three times to assess reproducibility. For grinding samples of feed sizes below 1000 μm, representative subsamples were obtained from the grinding products using a rotary sample divider (Retsch PT 100) prior to laser diffraction analysis.

#### 2.3.2. Single particle compression

The investigation of single particle breakage was conducted using a Retroline 10 kN compression unit from Zwick/Roell, Germany, for static applications. One hundred particles from the three selected size classes in crushing were subjected to a continuously increasing compressive load until breakage occurred, at which point the load was reduced to 30% of the maximum. The specific energy was calculated from the force-displacement diagram.

#### 2.3.3. Specific surface area

The specific surface area of the samples was determined by nitrogen adsorption using a BET-based analyzer (NOVA 2200, Quantachrome Instruments). Before measurement, all samples were thermally conditioned at 270 °C for two hours to remove adsorbed moisture and volatile surface species.

### 2.4. Data evaluations and theoretical background

In comminution, the efficiency of the process is mainly evaluated based on energy consumption for the grinding. In impact stressing, the specific comminution energy was determined by directly measuring the

power consumed by the impact mill during the grinding process, as given in Eq. (1), where the no-load power was measured as $P_0$. The specific comminution energy under compressive stress in the roller mills was determined by measuring the torque M, where $n_{roll}$ is the circumferential speed and $m_p$ is the mass of the sample (Eq.(2)).

$$E_{m,\ impact} = \frac{\int_{t_0}^{t_1} (P - P_0)dt}{m_p} \quad (1)$$

$$E_{m,\ compression} = \frac{2\pi n_{rolls} \int_{t_0}^{t_1} (M - M_0)dt}{m_p} \quad (2)$$

Since not only the particle size but also the particle size distribution influences the separation by flotation, the polydispersity index (PDI) was used as a measure of the width of the particle size distribution and thus the degree of size heterogeneity within a sample, given in Eq (3).

$$Polydispersity\ index = \frac{x_{90} - x_{10}}{x_{50}} \quad (3)$$

Based on the measured and calculated specific energy, the size specific energy, SSE, is defined as the ratio of the specific input energy ($E_m$) to the mass fraction of newly generated fines below the reference size ($P_{xr}$), quantifies the energy required to produce particles smaller than the defined size, shown in Eq. (4). Lower SSE values indicate higher comminution efficiency [38]. Another parameter used to evaluate the comminution efficiency is the energy utilization, which is calculated based on the new specific surface area, ΔS, and the specific energy, $E_m$, as presented in (Eq. (5)).

$$Size\ specific\ energy\ (SSE) = \frac{E_m}{P_{xr}} \quad (4)$$

$$Energy\ utilization\ (EU) = \frac{\Delta S}{E_m} \quad (5)$$

The evaluation of cumulative specific energy, size-specific energy, and energy utilization, as well as the measurements used to summarize and compare comminution performance, are described in detail in the Results and Discussion section in conjunction with the corresponding figures.

## 3. Results and discussion

### 3.1. One-pass milling

The first step in designing the comminution chain was to study the behavior of particles under impact and compressive stress, excluding repeated breakage events. Three different size classes were crushed, and the breakage behavior of the milling products was compared in terms of fineness and energy consumption. Based on the results, grinding was conducted only under compressive stress.

#### 3.1.1. Crushing

This study focused on the comminution of slag particles. The first step involved crushing using an impact mill and a roller crusher to compare the efficiency of impact versus compressive stressing. The particle size distributions and the specific comminution energies corresponding to the three feed size classes after crushing under impact and compressive stressing are shown in Fig. 2. A typical characteristic of impact stressing was the broader particle-size distribution, which could also be observed from the polydispersity index (PDI) as in Eq.(3) and presented in Table 3. Within the context of liberation, lower PDI values indicated a narrow distribution, which improves flotation selectivity [12]. Impact stressing created multiple fracture points, producing a mixture of fine and coarse particles in the product [39]. This behavior was evident for the largest feed size ($x_{50}$ = 9.4 mm, PDI = 4.3) but less pronounced for other size classes (PDI = 1.7 and 1.6). In contrast, compressive stressing involved the gradual application of pressure, generating more uniform products —typically with PDIs below 1.0 —confirming the narrower particle-size distribution associated with multiple stress events.

Comparing the PDI values for different size classes with varying roller-mill gap sizes revealed that smaller gap sizes (<30% of the $x_{50,\ feed}$) produced higher PDI values and thus broader distributions, likely due to increased fine-particle generation and local agglomeration. To clarify this behavior, the relationship between product particle size distribution, specific comminution energy, and breakage mechanism was further examined (Fig. 2).

Specific comminution energies for the impact mill and roller crusher have been measured and calculated based on the Eqs. (1) and (2) given in the previous section. These values with their standard deviations are presented in Table 4.

A comparison of the product particle sizes ($x_{50}$) for the three feed size classes showed similar median sizes for all impact stressing experiments. Although a finer product was expected for finer feed sizes at the same

**Table 3**
Polydispersity index (PDI) values for three feed size classes (crushing) under impact and compressive stress at different roller gap settings.

| Stress type | Impact | Compression | | | |
|---|---|---|---|---|---|
| $x_{50,\ feed}$ (mm) | PDI (-) | Gap size: 20% of $x_{50}$ | Gap size: 30% of $x_{50}$ | Gap size: 40% of $x_{50}$ | Gap size: 50% of $x_{50}$ |
| 9.4 | 4.3 | 1.9 | 1.1 | 0.7 | 0.5 |
| 4.6 | 1.7 | 1.0 | 1.5 | 0.9 | 0.8 |
| 1.7 | 1.6 | 1.7 | 1.0 | 1.0 | 0.9 |

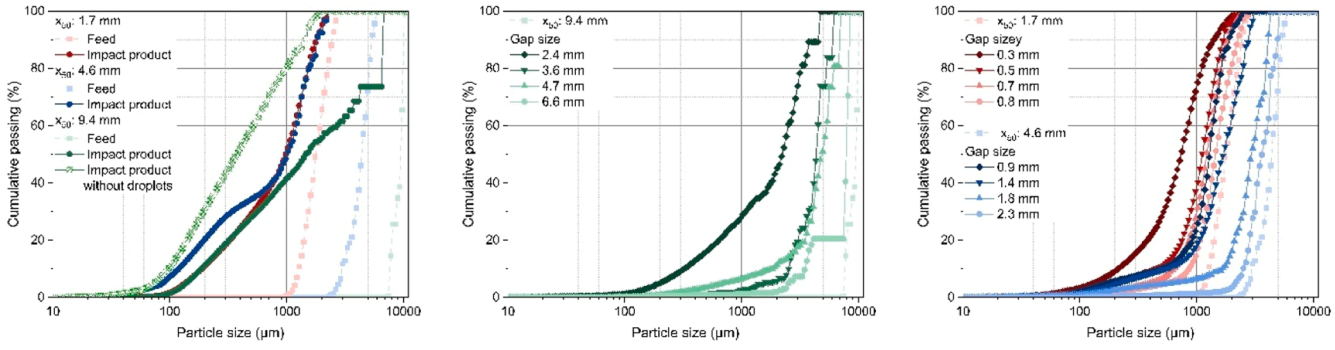


a) b) c)

**Fig. 2.** Cumulative passing of the milling product of the three feed size classes with specific breakage energy: a) Impact mill; b) Roller crusher with variation of gap size and feed of $x_{50}$: 9.4 mm; c) Roller crusher with variation of gap size and feeds of $x_{50}$: 1.7 and 4.6 mm.

**Table 4**
Specific comminution energy for the three defined feed sized using impact and compression.

| Stress type $x_{50,\ feed}$ (mm) | Specific energy (J/g) Impact | Specific energy (J/g) Compression | | | |
|---|---|---|---|---|---|
| | | Gap size: 20% of $x_{50}$ | Gap size: 30% of $x_{50}$ | Gap size: 40% of $x_{50}$ | Gap size: 50% of $x_{50}$ |
| 9.4 | 8.3 ± 5.6 | 0.76±0.34 | 0.67±0.13 | 0.62±0.13 | 0.31±0.09 |
| 4.6 | 8.2 ± 7.6 | 1.76±0.84 | 1.16±0.55 | 1.09±0.61 | 0.69±0.33 |
| 1.7 | 8.3 ± 5.4 | 1.44±0.66 | 1.31±0.64 | 1.12±0.62 | 0.77±0.07 |

specific input energy (8.3 J/g), only an 8–10% reduction in $x_{50}$ was observed. Assuming each particle was stressed once, the stress intensity depended on the particle kinetic energy, which is proportional to the square of the tip speed ($v_{tip}$). Because the tip speed was constant across all experiments (21.1 m/s), the specific breakage work depended only on the tip speed, as shown in Eq. (6).

$$E_{cs,spec} = Stress\ Number \times Stress\ Intensity \propto Stress\ Number \times v_{tip}^{\ 2} \quad (6)$$

In comparison with the calculated specific input energy (8.3 J/g) obtained from power measurements of the mill and using Eq. (2), the specific breakage work accounted for only about 4% of that value, highlighting the low energy efficiency of impact milling due to single-event stressing and incomplete energy utilization, especially for the 1.7 mm feed class. Another unexpected breakage behavior was in the largest feed class ($x_{50}$ = 9.4 mm). In spite of similar median sizes, in this size impact stress produced a considerable number of coarse fragments ($x_{90}$ > 7 mm). Detailed inspection of the products (Fig. 3a) revealed that these coarse particles were primarily metallic droplets remaining within the slag matrix. Because these droplets underwent plastic deformation rather than brittle breakage, the applied impact energy was sufficient to detach but not grind them. To remove the effect of droplets, the particle size distribution was recalculated for feed size of $x_{50}$ = 9.4 mm and showed in Fig. 2a with a different symbol.

A comparative analysis under compressive stressing using the roller crusher showed that reducing the roller-gap size produced finer grinding products (Fig. 2b). In contrast to impact stressing, decreasing the feed size under compression also resulted in a finer product, indicating a stronger dependence on gap control and compression intensity. An exceptional behavior was observed for the feed class with $x_{50}$ = 9.4 mm, again attributed to metallic droplets. The coexistence of ductile metallic inclusions and brittle silicate phases led to heterogeneous stress absorption, where metallic droplets acted as local energy loss, reducing overall breakage efficiency in this size fraction and altering the particle size distribution (PSD) similar to impact stressing.

A comparison between impact and compressive stressing revealed pronounced differences in both the specific breakage work and the dominant fracture mechanisms (Fig. 2). Under slow, single-particle compression, the specific breakage work for slag particles typically ranged between 0.01 and 0.1 J/g, representing the minimum energy required to break individual particles once. In contrast, compression in roller mill required specific breakage energy values varying from approximately 0.1 to 2.5 J/g, depending on the feed size class and the applied roller gap (Fig. 2b). The significantly higher energy range in the roller mill reflected the transition from a single breakage event to multiple breakage events, in which repeated stressing and interparticle contacts contribute to cumulative energy dissipation, as also observed by Böttcher et al. in a rigidly mounted roller mill [40].

Another aspect influencing the product size was the type of stressing and the corresponding breakage mechanism. Three primary breakage mechanisms were identified—shattering, cleavage, and chipping (Fig. 3b). In impact milling, the dominant mechanism was shattering (body breakage), a catastrophic fracture process where particles disintegrate into multiple fragments once the applied stress exceeds their elastic limit [37]. At a tip speed of approximately 21 m/s, the breakage patterns were consistent with fragmentation patterns reported by Miao at particle-impact velocity of around 13 m/s [41]. Under impact, strain energy accumulated faster than it could be released, resulting in simultaneous crack initiation and propagation throughout the particle. This explains the predominance of fine fragments and the wide PSD observed in impact stressing.

During slow compression in the roller mill, lower-intensity regions were formed with cleavage and chipping as the main mechanisms. Cleavage occurs when the applied stress is sufficient to initiate cracks along planes of weakness but not enough to cause total disintegration. The result is a few large fragments that separate cleanly along grain boundaries or phase interfaces. Chipping, the least energetic mode, involves the detachment of small surface fragments or corners due to repeated, low-intensity contact or shear stresses. It becomes prevalent during secondary stressing or attrition phases, particularly when energy input decreases or residual stresses remain after initial breakage [42].

Overall, the combined evidence from Fig. 2 indicates that breakage under both impact and compressive stressing is governed by an interplay of shattering, cleavage, and chipping, influenced by feed size, slag heterogeneity, and stress repetition. In compression, multiple contact points and extended stress duration favor cumulative cleavage and chipping events, while in impact, the high strain rate induces predominant shattering followed by limited secondary cleavage. This hybrid fracture behavior explains the broad PSDs and energy variability observed across feed sizes and underscores the importance of phase composition and mechanical contrast in optimizing slag comminution. Additionally, the observed differences in breakage behavior between impact and compressive stressing are strongly influenced by the heterogeneous microstructure of the slag, particularly the coexistence of ductile metallic inclusions and brittle ceramic phases. While phase-specific mechanical properties such as microhardness, fracture toughness, and interfacial bonding strength are expected to play a decisive role in these mechanisms, their quantitative assessment on microscale

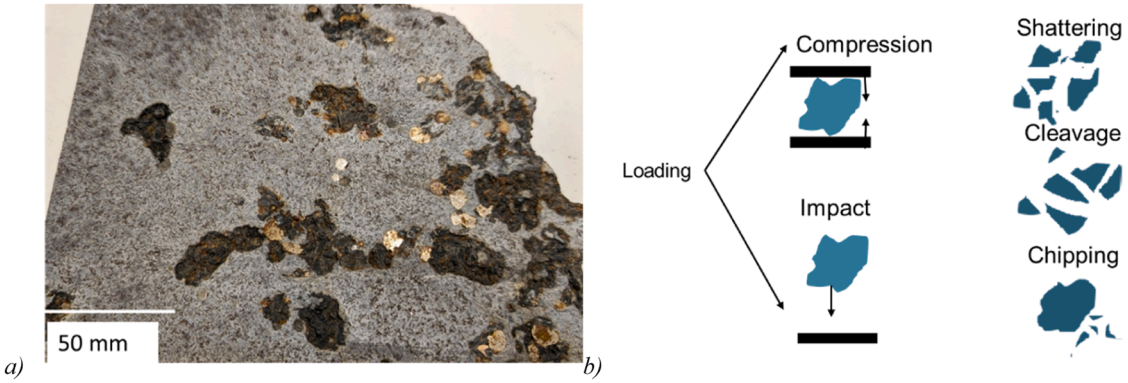


**Fig. 3.** a) Cross-section of the slag showing metallic droplets; b) Most frequent breakage mechanism under impact and compressive stress.

requires dedicated micromechanical characterization beyond the scope of the present work. The focus of this study is therefore placed on the development and evaluation of an energy-efficient comminution process chain—centered on roller-mill operation—rather than on phase-scale mechanical property determination.

Kinetic interpretation using the Austin population balance framework

To complement the particle size distribution (PSD) and energy-based evaluation, the comminution behavior was interpreted within the framework of the classical population balance model for batch grinding as formulated by Austin, Klimpel and Luckie [43]. In its differential form, the model describes the time-dependent evolution of the mass fraction $W_i(t)$ in size class $i$ as

$$\frac{dw_i(t)}{dt} = -S_i W_i(t) + \sum_{j=i+1}^{n} b_{ij} S_j W_j(t), \; n \geq i \geq 1 \tag{7}$$

where $S_i$ is the selection function (rate of breakage of particles in size class $i$) and $b_{i,j}$ is the breakage distribution function describing the fragment size distribution generated from the breakage of particles in class $j$, given in Eq. (7). The selection function is commonly expressed in empirical form in Eq. (8)

$$S_i = a \left(\frac{x_i}{x_0}\right)^{\alpha} \tag{8}$$

with fitting parameters, a and α, while the cumulative breakage function is often represented by a two-term power-law expression:

$$B_{i,j} = \phi \left(\frac{x_{i-1}}{x_j}\right)^{\mu} + (1-\phi)\left(\frac{x_{i-1}}{x_j}\right)^{\nu} \tag{9}$$

with material-dependent parameters ϕ, υ, and μ in Eq. (9).

In the present study, the crushing experiments (impact mill and roller crusher) represent single-stress-event breakage rather than continuous time-dependent batch grinding. Therefore, classical time-based rate constants $S_i$ (in $s^{-1}$) cannot be determined without introducing artificial residence-time assumptions. The comparison between stressing modes is therefore based on breakage outcome per stress event rather than grinding time.

To provide a kinetic descriptor consistent with the Austin framework, an effective first-order selection parameter was defined for the top size class (defined here as the coarse fraction represented by $x_{10}$):

$$S_i^{event} = -\ln\left(\frac{W_{i,\,product}}{W_{i,\,feed}}\right) \tag{10}$$

where $W_{i,\,feed}$ and $W_{i,\,product}$ denote the mass fractions of the top size class before and after one stress event, given in Eq. (10). This parameter represents the effective breakage probability per stress event and allows a direct comparison between impact and compressive stressing modes without invoking time-dependent assumptions.

Particle shape was analyzed using dynamic image analysis. Volume-weighted median circularity and aspect ratio were evaluated for all feed sizes and stressing conditions. Circularity exhibited a clearer and more systematic dependence on stressing mode than aspect ratio. Circularity is therefore presented as the primary morphological descriptor.

To provide independent comminution indices beyond PSD and energy analysis, the breakage behavior was evaluated using (i) an Austin-type event-based selectivity parameter and (ii) particle shape descriptor, circularity, obtained from dynamic image analysis.

The event-based selectivity, calculated from the logarithmic reduction of the feed-defined top fraction ($>x_{10,\,feed}$) is shown in Fig. 4a. as the top size is $x_{10}$ selected to avoid the uncertainties in the measurements and the possible dust remaining in the samples. For the 1.7 mm feed, compressive stressing exhibits a clear gap-dependent decrease in selectivity, with the 20% gap condition showing the highest breakage intensity. For the 4.6 mm and 9.4 mm feeds, impact and compression conditions lead to complete disappearance of the coarse fraction within experimental resolution, demonstrating high stressing intensity. Larger gaps preserve measurable coarse material, confirming that gap ratio governs compressive stress intensity.

The corresponding particle shape analysis (Fig. 4b) reveals systematic differences in circularity. Impact stressing consistently increases circularity across different feed size, indicating isotropic fracture and fragment rounding. In contrast, compression produces gap-dependent behavior, with small gaps generating angular fines and larger gaps promoting partial rounding of coarse particles. Aspect ratio trends were less systematic, whereas circularity provided a more consistent morphological indicator across conditions.

The combined evaluation of PSD evolution, energy utilization, event-based selectivity, and circularity demonstrates internally consistent trends across independent comminution descriptors. These descriptors provide complementary perspectives on stressing behavior without relying solely on PSD or energy metrics.

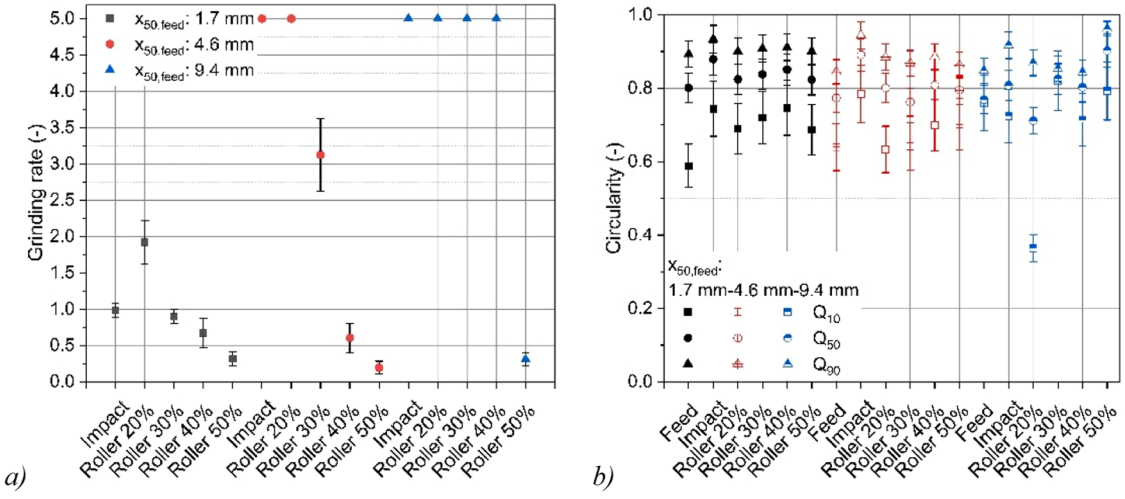


**Fig. 4.** a) Grinding rate of the top fraction ($>x_{10,feed}$) for impact and compressive stressing; For experiments in which the coarse fraction was completely removed ($W_i$=0), the grinding rate could not be determined, as the logarithmic expression ($\ln(0/W_{i,\,feed})$ is undefined. For visualization purposes only, an arbitrary value of 5 was assigned in the diagram to clearly identify these conditions. This value is not a measured or calculated parameter but exclusively a graphical indicator of complete coarse particle removal.

### 3.1.2. Grinding

For the grinding tests, three size classes were milled in a rigidly-mounted roller mill while varying the roller gap size (Table 2b). Reducing the roller gap size and decreasing the feed size produced finer particles, consistent with findings of Böttcher and colleagues [40,36]. As shown in Fig. 5, at smallest gap settings (30% of the feed $x_{50}$), grinding produced 30–70% particles in the 30–100 μm range, suitable for flotation and improving yield by up to 10% [12].

### 3.1.3. Evaluation of crushing and grinding efficiency using size-specific energy

The energy efficiency of different comminution modes was evaluated using size-specific energy (SSE) Eq. (4), for a cut size of 100 μm, corresponding to the target flotation feed size.

Under impact stressing, SSE values exceeded 100 J/g for all feed sizes as shown in Fig. 6a, confirming the low efficiency of impact crusher in directly achieving the target size. As the feed particle size decreased, most of the input energy was dissipated as heat rather than as breakage into fine particles. Nevertheless, impact crushing was beneficial for liberating metallic droplets from the slag matrix prior to compression stages, thereby simplifying downstream processing and avoiding roller damage.

In contrast, compression crushing produced a wide range of SSE values (Fig. 6b) demonstrating that energy efficiency strongly depended on roller-gap setting and feed size. In general, reducing the feed size and gap size, lower SSE values were reached in the roller crusher. At the largest gap size for the 9.4 mm feed, the lower SSE could be the result of the chipping mechanism in brittle phases. The narrow distribution of products under compression suggested that SSE for the target size was not a good indicator for the efficiency of the roller crusher. It should be noted that the measured specific input energies were subject to methodological limitations. For impact crushing, the energy values were derived from electrical power measurements after subtracting the no-load power, which provides only an indirect estimate of the actual impact energy. More accurate values would require direct measurement of particle velocities using high-speed imaging. In the roller crusher, substantial mechanical losses from the heavy rolls, their slight movements during milling, and the dual-drive motor system were considerably higher than in the rigidly mounted roller mill with one motor and rigid rollers. These losses increase the uncertainty of the measured power and complicate direct comparisons of energy efficiency between the two mills.

The size specific energy of grinding in the rigidly mounted roller mill (Fig. 6c) showed approximately a 30% decrease compared with values obtained in the roller crusher. SSE decreased from approximately 20 J/g to single-digit values as the relative gap size increased from 30 to 60%. The feed size did not play a significant role unlike in the roller crusher. Overall, SSE analysis across both crushing and grinding stages indicated that a multi-stage comminution circuit in an industrial scale offers the most energy-efficient route to achieve a flotation-ready product (< 100 μm). This conclusion is based on the combined evaluation of SSE and EU across stressing modes and gap configurations within the investigated parameter range. Future work should quantify stress–energy and correlate it with phase liberation behavior to support predictive process design. A better approach to compare the efficiency of different milling settings in crushing and grinding was the energy utilization (EU) as presented in Fig. 6d-f.

Although energy utilization provided a more fundamental basis for comparing comminution efficiency, this approach could not be applied directly to the initial crushing stage because surface area measurements obtained by BET were not sufficiently reproducible within the investigated crushed particle size range. Instead, the specific surface area (SSA) was estimated from the measured particle size distributions using a mass-weighted summation over individual size classes. To account for particle non-sphericity and the associated underestimation of external surface area inherent to purely geometric assumptions, a shape correction factor based on particle circularity was introduced. The resulting formulation is given in Eq. (11) where $w_i$ denotes the mass fraction of size class i, $d_i$ the representative particle diameter, ρ the material density, and $\varphi_i$ the circularity-based form factor. The measured true density of the slag used in this study was 2.92 g/cm³. The corresponding results are presented in Fig. 6.

$$SSA_{PSD,shape} = \sum_i \frac{6w_i}{\rho \varphi_i d_i} \tag{11}$$

Energy utilization (EU) was evaluated as a function of feed size and gap geometry for the impact mill, roller crusher, and rigidly mounted roller mill (Fig. 6). Because feed size and gap size represent continuous operational parameters, regression analysis was used to quantify systematic trends. Model significance was assessed by ANOVA of the fitted models. Detailed regression parameters are provided in Fig. 6.

EU in impact mill increases with increasing median feed size, following the logarithmic trend shown in Fig. 6d The regression explains the majority of the variance ($R^2 \approx 0.96$). However, due to the limited number of feed-size levels (n = 3), the regression ANOVA does not reach statistical significance ($p > 0.05$). The observed relationship should therefore be interpreted as a strong descriptive trend constrained by statistical power. No inferential conclusions are drawn solely from this regression.

For the roller crusher (Fig. 6e), EU decreases systematically with increasing gap size. The fitted power-law model is highly significant ($p < 0.0001$) and explains approximately 94% of the observed variance.

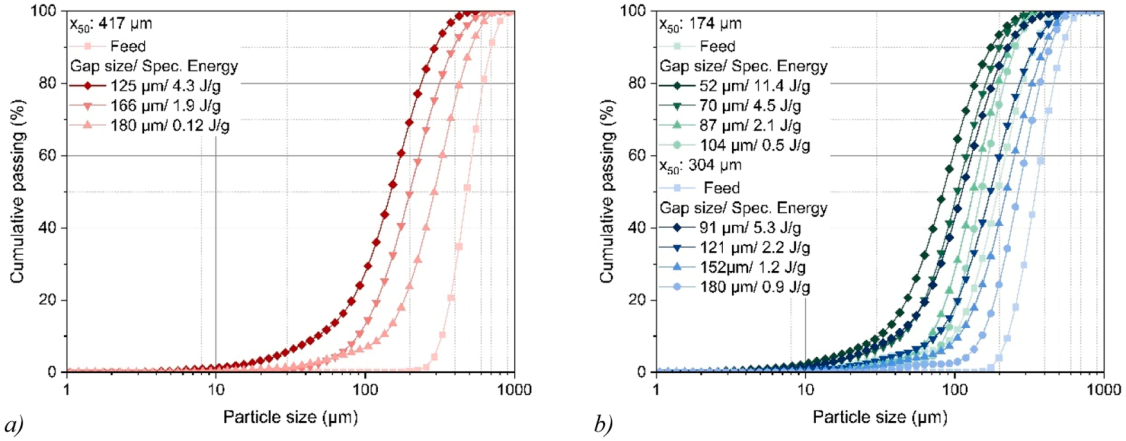


**Fig. 5.** Particle size distribution of grinding in the rigidly-mounted roller mill with varying gap sizes and feed size classes: a) Feed size of 417 μm; b) Feed sizes of 304 and 174 μm.

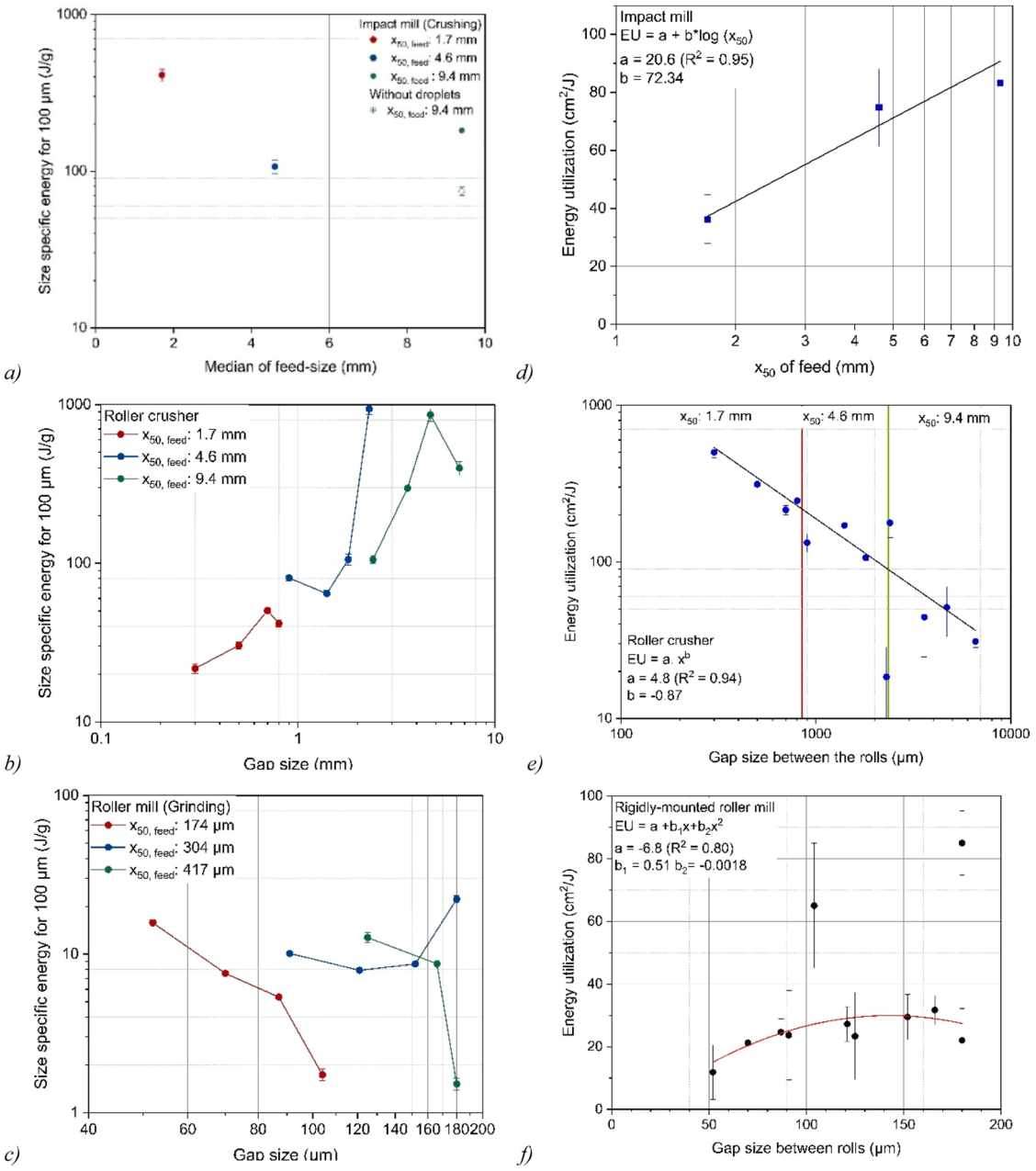


**Fig. 6.** Size-specific energy (SSE) at 100 µm and energy utilization for a, e) Impact mill; b, d) Roller crusher; c, f) Roller mill for grinding as single breakage events.

This confirms a statistically robust inverse dependence of EU on gap geometry. Within the investigated parameter range, gap size is therefore the dominant variable governing EU in roller crushing.

In the rigidly-mounted roller mill (Fig. 6f), EU exhibits a non-linear dependence on gap size. The quadratic regression model is statistically significant ($p = 0.003$), with both linear and quadratic terms contributing significantly. The model explains approximately 81% of the variance, after exclusion of two clearly identifiable outliers at 60% relative gap for the two larger feed sizes; these points were excluded due to anomalous behavior associated with minimal mass transfer into the target size class and are documented in the revised figure caption. The curvature indicates an optimum EU at intermediate gap sizes within the investigated range. This statistical result suggests the existence of an optimal geometric stressing condition under the tested conditions. Furthermore, excessively narrow gaps increased friction, promoted partial particle-bed formation, and allowed fines to shield coarse particles—each contributing to additional energy losses [44].

The finest feed (174 µm) showed comparatively low EU values, reflecting reduced efficiency as the product approached the target cut size due to limited fracture probability. As feed size decreased, the number of pre-existing defects within the particles was reduced, requiring higher stress energy for continued breakage [45,46].

To sum up, across the three stress modes, distinct dependencies emerge: Impact milling shows a strong, though statistically underpowered, increase in EU with feed size. Roller crushing exhibits a highly significant inverse dependence of EU on gap size. Roller milling demonstrates a statistically significant non-linear optimum in gap geometry. These results demonstrate that energy utilization is controlled by the interaction between stress mode, particle size regime, and geometric stressing conditions. Continuous regression analysis provides a more mechanistically meaningful interpretation than categorical comparison alone and directly addresses the reviewer's request for statistical validation.

### 3.2. Multiple-pass grinding (continuous)

Two continuous grinding strategies were examined in the rigidly mounted roller mill to achieve a flotation-ready particle size (< 100 μm). These approaches, illustrated in Fig. 1b, demonstrate the potential for process upscaling and optimization of cumulative energy use during comminution.

#### 3.2.1. Series operation

In the series configuration, no sieving was performed between passes. Particle size evolution was tracked by laser diffraction, and grinding continued until $x_{90} < 100$ μm, corresponding to the flotation-ready size fraction. The roller gap size) was defined as the ratio of instantaneous gap to the median feed size ($x_{50}$) measured after each stress event. After each pass, Δs was recalculated based on the newly measured $x_{50}$ of the milling product and the relative gap size set for that row of experiments, for instance 30%. Fig. 7 shows the evolution of particle-size distribution for the feed class with $x_{50} = 174$ μm under relative gap sizes of 30 – 60%. The exact gap size implemented for each stress event is shown in the diagrams. The remaining datasets for other feed classes are provided in the Supplementary Material.

A consistent trend across all feed classes was that larger gap ratios (Δs ≥ 50%) required more stress events to reach the target size, because the increased gap between the rollers, increased the nipping angle between particles and rollers, and thus reduced efficient applied stress on the particles. Similar behavior was observed in previous study [36].

#### 3.2.2. Circuit operation

In the circuit mode, each pass was followed by sieving at 100 μm to separate the flotation-ready fraction. The retained coarse material was remixed with an equal mass of fresh feed and returned to the mill. Yield of each stress event was calculated based on the weight of the product under 100 μm as in Eq. (12).

$$Yield\ of\ circuit\ operation = \frac{Weight_{fines<100\ \mu m}}{Weight_{sample\ in\ each\ stress\ event}} \quad (12)$$

The roller gap (Δs) was maintained constant at 30% and 40% of $x_{50}$ of initial feed. The process was continued until three consecutive passes exhibited (i) constant feed size ($x_{50} \pm 2\%$) and (ii) a stable yield (±5%). This condition defined steady-state grinding, where input energy and particle breakage reached equilibrium as presented in Fig. 8a and b. Although only one target size was evaluated here, the same approach could be extended to coarser stages (e.g., crushing) by defining size-specific targets for each feed class. Fig. 8a illustrates the evolution of feed size ($x_{50}$) with successive stress events. Across all initial feed classes, $x_{50}$ decreased rapidly during the first two stress events and then plateaued, confirming that equilibrium was reachable after the fourth or fifth pass. The product yield (Fig. 8b) reached a constant range of approximately 10 wt.% for the coarse feeds ($x_{50} = 417$ and 304 μm) and 30–35 wt.% for the fine feed ($x_{50} = 174$ μm). The stabilization of yield supports the achievement of a steady-state (ss) or stationary condition, which is later used for the calculation of milling efficiency.

#### 3.2.3. Evaluation of energy efficiency in circuit and series operations

Determining the specific energy applied in series and circuit operation of roller mill was the key step in evaluating the efficiency of both approaches. Fig. 9a shows the evolution of specific energy across the relative gap sizes of the $x_{50}$ for the current stress event in series operation for the feed size of 174 μm. Depending on the feed particle size and the chosen relative gap setting, 3–6 stress events (S1-S6) were necessary to reach the target size of below 100 μm. The specific energy for the feed sizes of 304 and 417 μm are presented in the Supplementary Material. To

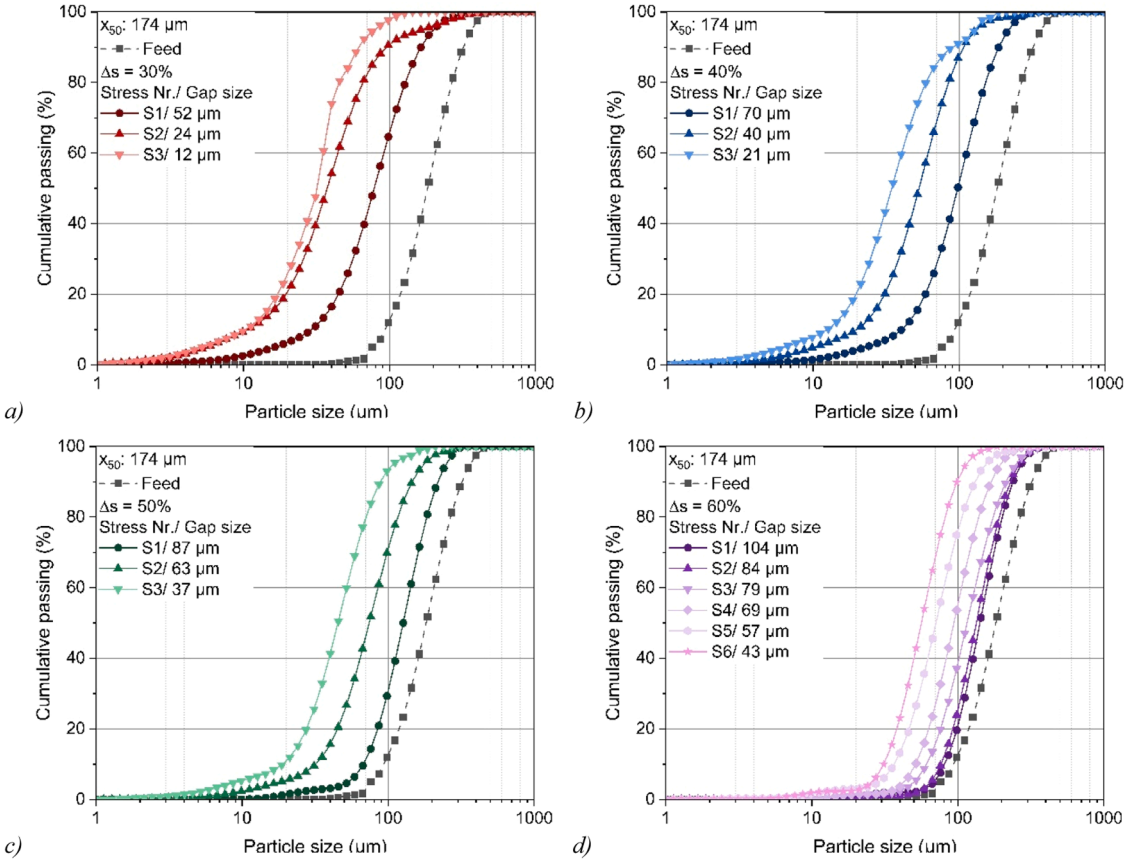


**Fig. 7.** Particle size distribution after multiple stressing events required to reach the target size of 100 μm for a feed with $x_{50} = 174$ μm, using relative gap sizes of a) 30%; b) 40%; c) 50%; d) 60% of $x_{50}$.

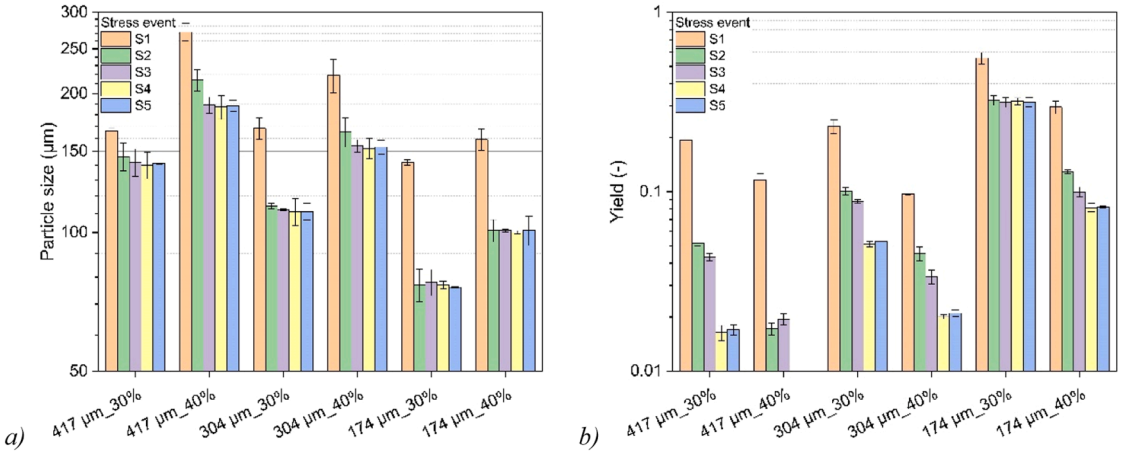


**Fig. 8.** Circuit operation: Effect of median feed size ($x_{50}$) and number of stress events S (number of passes) on a) median particle size; b) yield of < 100 µm product for each feed sizes.

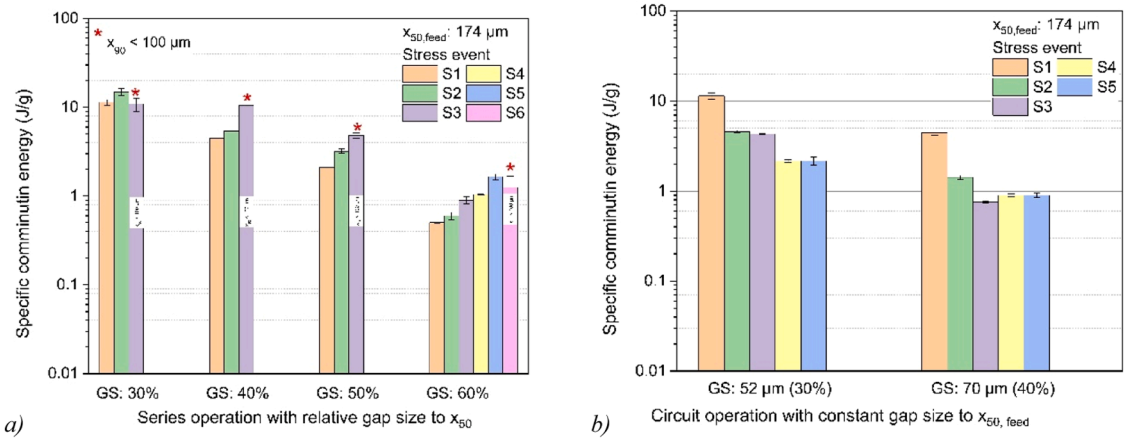


**Fig. 9.** a) Specific energy in series operation for $x_{50}$:174 µm at relative gap sizes of 30%, 40%, 50%, and 60% to the $x_{50}$ for the current stress event; b) Specific energy in circuit operation for $x_{50}$:174 µm at gap sizes of 52 and 70 µm (30% and 40%).

compare both operations, the specific energy for the first five stress events of the feed size of 174 µm with constant gap size of 52 and 70 µm (30 and 40%) in circuit operation is presented in Fig. 9b For all feed sizes, as a general trend in the roller mills, specific energy in the first stress event decreased markedly with increasing gap sizes for that feed size. In series operation, with increasing the relative gap size for each feed (30% to 60%) the number of stress events necessary to reach the target size of under 100 µm increased. Since, the gap size was adjusted after each stress event and the fines remained in the feed of next event, the specific energy increased, however, the cumulative specific stress for each relative gap size did not increase. One explanation is that at smaller gap sizes (30 and 40%), fines remained on the rollers, forming a particle bed and increasing the specific input energy, as for the 50 and 60% gap sizes, the produced fines were significantly smaller than the current gap size and could fall between the rolls without being stressed.

In the case of circuit operation, the first stress event had the highest specific energy consumption. With repeated stressing, the specific energy decreased continually as a result of material weakening, as observed in other works [40,25]. After reaching the steady state (the fourth stress event), the specific input energy did not change significantly, similar to the median feed size and yield observed in this stressing event, which indicated the number of weakened particles also remained almost constant.

For the evaluation of the series and circuit operations of the roller mill, both SSE for the cut size of 100 µm, presented in a and b, and the energy utilization illustrated in c and d were considered. To have a better representation of the influence of specific comminution energy, the SSE and EU were calculated using Eq. (13) and (14), with $\Sigma E_m$ as the cumulative specific comminution energy of the selected milling setting, and $S_{m,final\ stress\ event}$ the specific surface area of its final product. In circuit operation, Eq. (15), $E_{ss\ (steady\ state)}$ as the specific comminution energy, mass of product ($m_{p,ss}$), the specific surface area of the separated fines ($S_{m,ss,fines}$), in the steady state (fourth stress event) were used.

$$SSE_{series} = \Sigma E_{m,} SSE_{circuit} = \frac{E_{ss}}{m_{p,ss}} \tag{13}$$

$$EU_{series} = \frac{S_{m,final\ stress\ event} - S_{m,1st\ stress\ event}}{\Sigma E_m} \tag{14}$$

$$EU_{circuit} = \frac{S_{m,ss,fines} - S_{m,\ 1st\ stress\ event}}{E_{ss}\ /m_{p,\ ss}} \tag{15}$$

In the series operation, several stress events were required to reach the target size; therefore, the size-specific energy (SSE) values could only be calculated as a function of the cumulative specific energy ($\Sigma E_m$) of the selected setting. Fig. 10a shows a consistent decrease with increasing relative gap size for the same feed size. For all feed sizes, SSE declined from roughly 30–40 J/g at a relative gap size of 30% to below 10 J/g at a relative gap size of 60%. The decrease in SSE values indicates that wider gap sizes resulted in more energy-efficient grinding; however, the

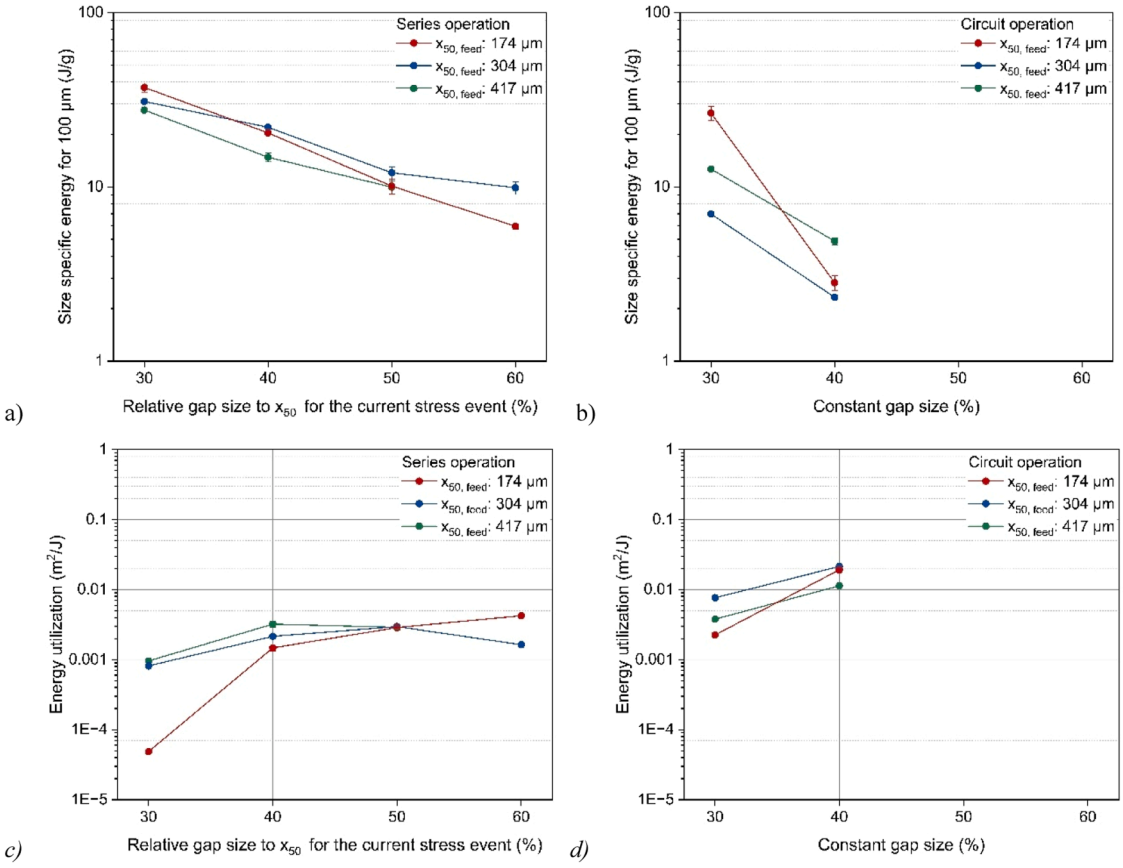


**Fig. 10.** Size specific energy and energy utilization for both series and circuit operations.

number of required stressed events increased, with an apparent preference for the relative gap size of 50% as the optimum balance between energy use and number of stress events. The finest feed ($x_{50}$ = 174 µm) exhibited the lowest SSE at large gaps, whereas the coarser feeds ($x_{50}$ = 304 and 417 µm) showed a more gradual decline, yet remained within a similar overall range. This indicates that breakage efficiency in series operation is governed mainly by gap size (compression intensity) rather than feed size.

In the circuit operation, due to the sieving step, products within the target size were obtained already after the first stress event. Therefore, for the calculation of SSE and EU, the specific energy was related only to one stress event and the yield of the product at the target size for that milling setting. To obtain a realistic view for a scalable operation, the values from the fourth stress event—where steady-state conditions were reached—were used. As mentioned in the Methods section, the gap sizes of 50% and 60% were excluded from the analysis because they produced only negligible amounts of fines in the target size range. As shown in Fig. 10b, the circuit operation produced distinctly lower SSE values overall, ranging approximately between 30 and 2 J/g, with a strong decrease as the gap size widened from 30 to 40%. The finest feed again required slightly higher specific energy at the narrowest gap, but differences among feed classes diminished at the wider setting, suggesting that steady state conditions minimize feed-size effects on overall energy demand.

In addition, size-specific energy (SSE) was evaluated for flotation-relevant size intervals (0–20, 20–50, 50–100, 100–200, and 200–350 µm) based on the measured particle size distributions and the specific energy of each stress event. In the crushing configurations (impact and parallel compressive stressing), the mass fraction transferred into these intervals was very small. As a consequence, fraction-resolved SSE values become numerically large but of limited physical significance, since only negligible amounts of material are produced in the flotation-relevant classes. Moreover, part of the applied energy under compressive stressing contributes to subcritical crack formation without immediate size reduction, preventing an unambiguous allocation of energy to a specific size interval. Therefore, fraction-based SSE analysis is discussed in detail only for the grinding in series operation of the rigidly mounted roller mill, where significant and quantifiable mass transfer into flotation-relevant fractions occurs.

Size-specific energy (SSE), as shown in Fig. 11, evaluated for flotation-relevant size intervals, classified as −20, 20–50, 50–100, 100–200, 200–350 µm, reveals a characteristic distribution across all feed sizes. The lowest SSE values are consistently observed in the intermediate fractions (20–50 and 50–100 µm), indicating that these size classes are generated most efficiently under controlled stressing. In contrast, both the fine fraction (0–20 µm) and the coarse fraction (200–350 µm) exhibit elevated SSE values. For fines, this behavior reflects the small mass fraction generated per stress event, resulting in high energy cost per gram. The high SSE in coarse fractions indicates insufficient breakage of resistant particles. Increasing gap ratio leads to greater variability and instability of fraction-resolved SSE, particularly at 60%, where only minor mass transfer into flotation-relevant fractions occurs. These results suggest that controlled grinding conditions may be more favorable for generating flotation-relevant size classes, whereas crushing-type stressing potentially appears to produce these fractions to a lesser extent under the investigated conditions. The energy utilization (EU) trends (Fig. 10c and d) complement these observations. In series operation (Fig. 10c), EU increased by nearly one order of magnitude from relative gap size of 30% to 50%, then leveled off or slightly declined at 60%. This implies that intermediate gaps (40–50%) favor effective energy-to-surface conversion by balancing particle breakage and frictional losses associated with fine particles remaining in the new feeds. For circuit operation (Fig. 10d), EU values were generally higher and more uniform across feed sizes, increasing steadily from 30 to 40%

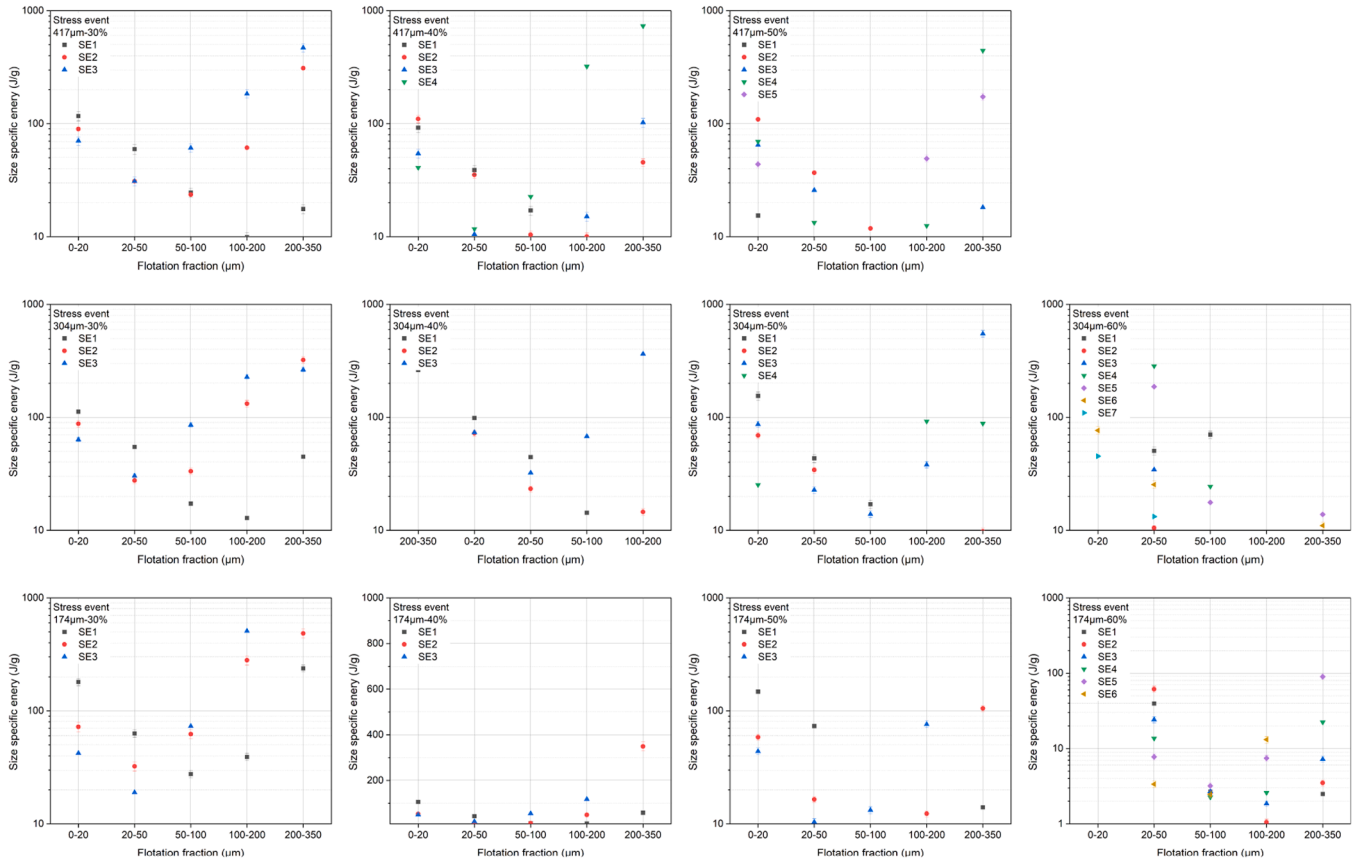


**Fig. 11.** Size specific energy for different feed sizes with the variations of gap size and stress events for different flotation classes (0–350 µm) with SE being the number of stress event in the circuit.

gap sizes, confirming that selective removal of fines enhances energy utilization.

In comparing the two continuous grinding modes, the circuit and series operations exhibit fundamentally different breakage environments, despite their similar layout. In the circuit mode, fines are removed after each pass and the feed is refreshed, allowing the milling parameters (circumferential speed and gap size) to remain constant. This promotes a stable single-particle stressing regime and prevents the formation of a particle bed. In contrast, the series operation continuously feeds the entire product of the previous pass into the next without classification. As the material becomes progressively finer, particle-bed formation becomes more likely, shifting the stressing conditions and requiring regular monitoring of the particle-size distribution to maintain appropriate milling parameters.

These mechanistic differences translate directly into performance outcomes. Circuit operation achieves higher energy efficiency because selective removal of fines minimizes redundant stressing. Series operation, however, generates more product in the target size than the sum of the products obtained in circuit operation at comparable stress events—up to three times more in some cases, except at the smallest gap sizes for the finest feed—while also eliminating the need for intermediate classification equipment. Overall comminution efficiency should therefore be evaluated not only by total energy input but also by the surface area generated per unit energy. Consistent with established stress models, multi-pass compression is most efficient when the roller-gap ratio is optimized, providing the best balance between energy use, controlled stressing conditions, and reliable production of flotation-ready particles. The present study provides an experimental comparison of stressing modes and operational parameters for lithium-bearing slag comminution. While systematic relationships between stress type, gap geometry, PSD evolution, energy utilization, and particle morphology are demonstrated, the development of a predictive mechanism model integrating mineralogical descriptors and phase-scale mechanical properties is beyond the scope of this work. Such modelling would require quantitative liberation metrics and micromechanical characterization not included in the current dataset. The trends identified here constitute an empirical basis for future model development.

## 4. Conclusion

This work presents a comprehensive assessment of the comminution behavior in lithium-bearing battery slags and proposes a scalable, energy-efficient process chain for their mechanical treatment. By comparing impact and compressive stressing modes across crushing and grinding stages, the study demonstrates that compression-based comminution in roller mills achieves higher energy efficiency, narrower particle size distributions, and more controlled breakage than single-impact stressing. Nevertheless, impact crushing remains beneficial for the early liberation of metallic inclusions from the slag matrix before subsequent fine grinding.

In the fine-grinding stage, multiple-pass compression using rigidly mounted roller mills effectively produced flotation-ready particles ($<$ 100 µm) when operated at an optimal relative gap ratio of approximately 40%. Among the continuous configurations tested, series operation required higher cumulative specific energy input, whereas circuit operation reduced total specific energy consumption by approximately 10–20% by minimizing redundant stressing of fines. Steady-state operation—defined by convergence of feed size, product yield, and specific energy—proved essential for evaluating true process efficiency and reproducibility.

From a process standpoint, both continuous strategies can be integrated into a staged grinding circuit. Series operation can serve as a

continuous crushing/coarse-grinding stage, allowing multiple roller mills to be arranged sequentially without intermediate classification. Once the slag properties are known, the median particle size at each step stabilizes, enabling the roller gaps to be fixed at roughly 50% of $x_{50,new}$, under such conditions, most fine particles pass directly to the next unit with minimal over-grinding. In contrast, circuit operation functions as a fine-grinding and liberation-control stage, where the target size is defined and separation techniques (such as sifters or magnetic separation) can be applied to isolate phase-specific fractions. This reduces gangue content and improves the efficiency of subsequent metal-recovery steps.

Energy efficiency in comminution should be assessed not solely by total input energy but by the applied breakage energy and the corresponding stress intensity. This criterion offers a mechanistic basis for designing adaptive dry-grinding circuits that optimize energy transfer, minimize over-grinding, and maintain sufficient liberation for flotation. The proposed process chain, integrating impact pre-crushing with staged roller-mill compression, provides a robust, low-maintenance, and industrially scalable approach for lithium recovery from engineered slags, contributing to sustainable recycling and circular resource utilization.

Future work should aim to quantify breakage kinetics and surface-generation rates under repeated stressing, correlate surface-area creation with phase-liberation efficiency, and develop predictive scale-up models linking stress intensity, throughput, and energy transfer. These insights will support the design of next-generation, energy-optimized roller-mill circuits for processing artificial engineered minerals.

## Funding

This research was funded by the German Federal Ministry of Education and Research within the project “PyroLith” (FKZ 03XP0336D).

## CRediT authorship contribution statement

**Sima Hellmers:** Writing – review & editing, Writing – original draft, Visualization, Validation, Software, Resources, Project administration, Methodology, Investigation, Formal analysis, Data curation, Conceptualization. **Hugo Lucas:** Methodology. **Bernd Friedrich:** Methodology, Funding acquisition. **Arno Kwade:** Writing – review & editing, Supervision, Project administration, Funding acquisition.

## Declaration of competing interest

The authors declare that they have no known competing financial interests or personal relationships that could have appeared to influence the work reported in this paper.

## Acknowledgments

Our thanks go to Marcel Möller and Bei Xing from the Institute of Particle Technology, Technische Universität Braunschweig for their support in the experimental part and editing.

## Supplementary materials

Supplementary material associated with this article can be found, in the online version, at doi:10.1016/j.rineng.2026.112294.

## Data availability

Data will be made available on request.

## References

[1] N. Shekhar Samanta, P.P. Das, S. Dhara, M.K. Purkait, An overview of precious metal recovery from steel industry slag: recovery strategy and utilization, Ind. Eng. Chem. Res. 62 (2023) 9006–9031, https://doi.org/10.1021/acs.iecr.3c00604.
[2] H. Shen, E. Forssberg, An overview of recovery of metals from slags, Waste Manag. 23 (2003) 933–949, https://doi.org/10.1016/S0956-053X(02)00164-2.
[3] L. Valderrama, J. Tapia, O. Pavez, M. Santander, V. Rivera, M. Gonzalez, Recovery of copper from slags through flotation at the Hernán videla lira smelter, Minerals 14 (2024) 1228, https://doi.org/10.3390/min14121228.
[4] G. Zhang, N. Wang, M. Chen, Y. Cheng, Comprehensive recovery of multisource metallurgical wastes: recycling nickel slag by aluminum dross with converter-slag addition, ISIJ Int 60 (2020) 1863–1871, https://doi.org/10.2355/isijinternational.ISIJINT-2019-670.
[5] F. Brandt, R. Haus, New concepts for lithium minerals processing, Miner. Eng. 23 (2010) 659–661, https://doi.org/10.1016/j.mineng.2010.03.021.
[6] A. Kwade, M. Möller, J. Müller, J. Hesselbach, S. Zellmer, S. Doose, J. Mayer, P. Michalowski, M. Powell, S. Breitung-Faes, Comminution and classification as important process steps for the circular production of lithium batteries, KONA 40 (2023) 50–73, https://doi.org/10.14356/kona.2023006.
[7] S. Windisch-Kern, A. Holzer, C. Ponak, H. Raupenstrauch, Pyrometallurgical lithium-ion-battery recycling: approach to limiting lithium slagging with the InduRed reactor concept, Processes 9 (2021) 84, https://doi.org/10.3390/pr9010084.
[8] M.T. Islam, U. Iyer-Raniga, Lithium-ion battery recycling in the circular economy: a review, Recycling 7 (2022) 33, https://doi.org/10.3390/recycling7030033.
[9] P.M. Tembo, C. Dyer, V. Subramanian, Lithium-ion battery recycling—a review of the material supply and policy infrastructure, NPG Asia Mater 16 (2024) 43, https://doi.org/10.1038/s41427-024-00562-8.
[10] S. Al-Asheh, A. Aidan, T. Allawi, F. Hammoud, H. Al Ali, M. Al Khamiri, Treatment and recycling of spent lithium-based batteries: a review, J. Mater. Cycles Waste Manag. 26 (2024) 76–95, https://doi.org/10.1007/s10163-023-01842-1.
[11] F. Steiner, A. Zgheib, M.H. Fischer, L. Büttner, A. Schmidt, S. Breitung-Faes, Situ hydrophobization of lithium aluminate particles for flotations by dry grinding in the presence of punicines, Minerals 14 (2024) 650, https://doi.org/10.3390/min14070650.
[12] S. Hellmers, H. Qiu, B. Yagmurlu, A. Kwade, Modifying milling parameters: impact on selective separation of lithium-rich phases in a thermodynamically designed battery slag, Clean. Eng. Technol. 24 (2025) 100857, https://doi.org/10.1016/j.clet.2024.100857.
[13] H. Li, H. Qiu, M. Ranneberg, H. Lucas, T. Graupner, B. Friedrich, B. Yagmurlu, D. Goldmann, J. Bremer, M. Fischlschweiger, Enhancing lithium recycling efficiency in pyrometallurgical processing through thermodynamic-based optimization and design of spent lithium-ion battery slag compositions, ACS Sustain. Resour. Manage. 1 (2024) 1170–1184, https://doi.org/10.1021/acssusresmgt.4c00064.
[14] H. Li, M. Ranneberg, M. Fischlschweiger, High-temperature phase behavior of Li2O-MnO with a focus on the liquid-to-solid transition, JOM 75 (2023) 5796–5807, https://doi.org/10.1007/s11837-023-06179-6.
[15] T. Schirmer, H. Qiu, H. Li, D. Goldmann, M. Fischlschweiger, Li-distribution in compounds of the Li2O-MgO-Al2O3-SiO2-CaO system—a first survey, Metals (Basel) 10 (2020) 1633, https://doi.org/10.3390/met10121633.
[16] A. Vanderbruggen, N. Hayagan, K. Bachmann, A. Ferreira, D. Werner, D. Horn, U. Peuker, R. Serna-Guerrero, M. Rudolph, Lithium-ion battery recycling–influence of recycling processes on component liberation and flotation separation efficiency, ACS EST Eng. 2 (2022) 2130–2141, https://doi.org/10.1021/acsestengg.2c00177.
[17] M. Javadi, C. Rachmawati, A. Wollmann, J. Weiss, H. Lucas, R. Möckel, B. Friedrich, U. Peuker, A.P. Weber, Enhancing lithium recovery from slag through dry forced triboelectric separation: a sustainable recycling approach, Minerals 14 (2024) 1254, https://doi.org/10.3390/min14121254.
[18] T.M. Campos, G. Bueno, V.A. Rodriguez, A.-C. Böttcher, A. Kwade, F. Mayerhofer, L.M. Tavares, Relationships between particle breakage characteristics and comminution response of fine iron ore concentrates, Miner. Eng. 164 (2021) 106818, https://doi.org/10.1016/j.mineng.2021.106818.
[19] E. Petrakis, V. Karmali, G. Bartzas, K. Komnitsas, Grinding kinetics of slag and effect of final particle size on the compressive strength of Alkali activated materials, Minerals 9 (2019) 714, https://doi.org/10.3390/min9110714.
[20] L.M. Tavares, R.P. King, Single-particle fracture under impact loading, Int. J. Miner. Process. 54 (1998) 1–28, https://doi.org/10.1016/S0301-7516(98)00005-2.
[21] H. Benzer, N.A. Aydogan, H. Dündar, Investigation of the breakage of hard and soft components under high compression: HPGR application, Miner. Eng. 24 (2011) 303–307, https://doi.org/10.1016/j.mineng.2010.09.012.
[22] S.L. Gay, A liberation model for comminution based on probability theory, Miner. Eng. 17 (2004) 525–534, https://doi.org/10.1016/j.mineng.2003.11.012.
[23] W.J. Kenny, E.L. Piret, Slow compression crushing of single particles of glass, AIChE J. 7 (1961) 199–202, https://doi.org/10.1002/aic.690070207.
[24] L.M. Tavares, M.C. Cerqueira, Statistical analysis of impact-fracture characteristics and microstructure of industrial Portland cement clinkers, Cem. Concr. Res. 36 (2006) 409–415, https://doi.org/10.1016/j.cemconres.2005.09.012.
[25] L.M. Tavares, R.P. King, Modeling of particle fracture by repeated impacts using continuum damage mechanics, Powder Technol. 123 (2002) 138–146, https://doi.org/10.1016/S0032-5910(01)00438-7.
[26] S.C. Chelgani, M. Parian, P.S. Parapari, Y. Ghorbani, J. Rosenkranz, A comparative study on the effects of dry and wet grinding on mineral flotation separation–a

review, J. Mater. Res. Technol. 8 (2019) 5004–5011, https://doi.org/10.1016/j.jmrt.2019.07.053.
[27] S. Luukkanen, A. Tanhua, Z. Zhang, R. Mollehuara Canales, I. Auranen, Towards waterless operations from mine to mill, Miner. Eng. 187 (2022) 107793, https://doi.org/10.1016/j.mineng.2022.107793.
[28] T. Napier-Munn, Is progress in energy-efficient comminution doomed? Miner. Eng. 73 (2015) 1–6, https://doi.org/10.1016/j.mineng.2014.06.009.
[29] V. Deniz, The effects on the grinding parameters of chemical, morphological and mineralogical properties of three different calcites in a Hardgrove mill, Miner. Eng. 176 (2022) 107348, https://doi.org/10.1016/j.mineng.2021.107348.
[30] C. Liu, Z. Chen, Y. Mao, Z. Yao, W. Zhang, W. Ye, Y. Duan, Q. Xie, Analysis and optimization of grinding performance of vertical roller mill based on experimental method, Minerals 12 (2022) 133, https://doi.org/10.3390/min12020133.
[31] S.M. Mehra, Slag grinding by roller press—major issues, Int. J. Miner. Process. 53 (1998) 87–97, https://doi.org/10.1016/S0301-7516(97)00059-8.
[32] K. Schönert, U. Sander, Shear stresses and material slip in high pressure roller mills, Powder Technol. 122 (2002) 136–144, https://doi.org/10.1016/S0032-5910(01)00409-0.
[33] M. Tobaben, A. Kwade, Fine grinding of pyrometallurgical battery slag and its influence on lithium dissolution, Miner. Eng. 216 (2024) 108879, https://doi.org/10.1016/j.mineng.2024.108879.
[34] A. Wikedzi, T. Leibner, T. Fraszcrak, U.A. Peuker, T. Mutze, Comminution characteristics of lithium bearing mica ores from different devices, TJET 39 (2020) 21–31, https://doi.org/10.52339/tjet.v39i1.516.
[35] H. Qiu, H. Li, M. Fischlschweiger, M. Ranneberg, T. Graupner, H. Lucas, C. Stallmeister, B. Friedrich, B. Yagmurlu, D. Goldmann, Valorization of lithium containing slags from pyrometallurgical recycling route of spent lithium-ion batteries: the enrichment of γ-LiAlO2 phase from thermodynamic controlled and modified slags, Miner. Eng. 217 (2024) 108918, https://doi.org/10.1016/j.mineng.2024.108918.
[36] A.-C. Böttcher, C. Thon, G. Fragnière, A. Chagas, C. Schilde, A. Kwade, Rigidly-mounted roll mill as breakage tester for characterizing fine particle breakage, Powder Technol. 383 (2021) 554–563, https://doi.org/10.1016/j.powtec.2021.01.055.
[37] Schönert, K.; Grundlagen zur Feinzerkleinerung, Preprints GVC-Dezembertagung 1993,. Feinmahl- und Klassiertechnik, Köln 02.-03.12.1993, GVC-VDI-Gesellschaft.
[38] G.R. Ballantyne, W. Peukert, M.S. Powell, Size specific energy (SSE)—energy required to generate minus 75 μm material, Int. J. Miner. Process. 136 (2015) 2–6, https://doi.org/10.1016/j.minpro.2014.09.010.
[39] H. Rumpf, Die einzelkornzerkleinerung als grundlage einer technischen zerkleinerungswissenschaft, Chemie. Ingenieur. Technik. 37 (1965) 187–202, https://doi.org/10.1002/cite.330370303.
[40] A.-C. Böttcher, D. Beusen, A. Lüddecke, A. Overbeck, C. Schilde, A. Kwade, Single and multiple breakage events in fine particle breakage testing with a rigidly-mounted roll mill, Miner. Eng. 178 (2022) 107390, https://doi.org/10.1016/j.mineng.2021.107390.
[41] C. Miao, S. Xu, P. Wang, Dynamic breakage of quartz glass sphere subjected to impact loading, in: Rock Dynamics: Progress and Prospect, 1, CRC Press, London, 2022, pp. 280–285, https://doi.org/10.1201/9781003359142-45.
[42] P. Semsari Parapari, M. Parian, J. Rosenkranz, Breakage process of mineral processing comminution machines – an approach to liberation, Adv. Powder Technol. 31 (2020) 3669–3685, https://doi.org/10.1016/j.apt.2020.08.005.
[43] L.G. Austin, R.C. Klimpel, A note on the prediction of specific rates of breakage for an equilibrium ball charge, Powder Technol. 43 (2) (1985) 199–201, https://doi.org/10.1016/0032-5910(85)87015-7.
[44] W. Xie, Y. He, Y. Wang, Y. Zhang, J. Yu, S. Wang, K. Li, Effect of fine particles on the breakage behavior of coarse coal in the Hardgrove mill, Int. J. Coal Prep. Util. 37 (2017) 326–338, https://doi.org/10.1080/19392699.2016.1183659.
[45] Y. Reichardt, K. Schönert, Interpartical breakage on fine hard materials by single and multiple compression, Chem. Eng. Technol. 26 (2003) 191–197, https://doi.org/10.1002/ceat.200390028.
[46] R. Weichert, Theoretical prediction of energy consumption and particle size distribution in grinding and drilling of brittle materials, Part Syst. Charact. 8 (1991) 55–62, https://doi.org/10.1002/ppsc.19910080111.